Molecular Vision 2026; 32:120-129 <http://www.molvis.org/molvis/v32/120>
Received 11 August 2025 | Accepted 18 February 2026 | Published 20 February 2026

Analysis of retinal ganglion cell subtypes across six different inbred mouse strains

Su-Ting Lin, Fangyu Lin, Jiaxing Wang, Eldon E. Geisert

Department of Ophthalmology, Emory University, Atlanta GA

Purpose: Retinal ganglion cells (RGCs) are the principal conduits responsible for propagating visual stimuli from the retina to visual centers in the brain. The loss of RGCs leads to visual deficits following trauma or in diseases such as glaucoma. Mouse models are consistently used to investigate root causes for RGC loss. This study quantifies the total number of RGCs and selected RGC subtypes across six strains of inbred mice used in ophthalmic research.

Methods: Six mouse strains (C57BL/6J, BALB/cByJ, 129X1/SvJ, A/J, CBA/CaJ, and CAST/EiJ) were selected to represent genetic diversity across the mouse genome. Normal retinas were immunostained for POU6F2, BRN3A, SATB2, OPN4, SMI32, and TO-PRO-3. Cells positively labeled for POU6F2, BRN3A, and SATB2 were quantified using an automated deep learning tool, RGCode. Cells labeled with OPN4, SMI32, and TO-PRO-3 were quantified using the Fiji software.

Results: We found statistically significant differences in the quantity (Mean±SEM) and percentage of different RGCs across the inbred mouse strains. The total number of RGCs per retina ranged from 39,961±838 in CAST/EiJ to 53,872±1864 in 129X1/SvJ ($p<0.005$). Global BRN3A counts ranged from 34,572±494 in CAST/EiJ to 44,253±798 in C57BL/6J ($p<0.005$). SATB2 counts ranged from 9944±384 in BALB/cByJ to 15,872±1196 in CBA/CaJ ($p<0.005$). OPN4 density ranged from 110±7 cells/mm^2 in CAST/EiJ to 164±13 cells/mm^2 in 129X1/SvJ ($p<0.05$). Differences in SMI32 density were not significant across all strains, with densities ranging from 183±14 cells/mm^2 in A/J to 279±12 cells/mm^2 in C57BL/6J (not significant).

Conclusions: There is a significant variation in total RGC counts and RGC subtypes across the different mouse strains. When working with different strains of mice, it is important to consider this strain-based variation before drawing conclusions from experimental data.

Experimental mouse model systems are commonly used to study retinal diseases affecting human populations. The inbred strains used in these model systems have the distinct advantage of providing a constant genetic background from one individual to another. The downside is that there are significant differences between different inbred strains of mice that can complicate the interpretation of the results depending upon the specific mouse strain used. In vision research, differences in retinal ganglion cell (RGC) number or in the proportion of specific RGC subtypes may have dramatic effects on the interpretation of the results. Even genetic drift or environmental factors within a single mouse strain C57BL/6 can result in significant differences in RGC number. For example, differences were found between the American and Italian colonies of C57BL/6J mice [1]. There are also differences between C57BL/6J mice from two Jackson Laboratory colonies [2].

The analysis of RGCs is further complicated by the approaches used to count RGC number (see Schlamp et al. [3]). Studies have estimated the number of RGCs by sampling areas of the optic nerve to determine axon density and then calculating the total number of axons in the entire nerve [1,2]. Other studies have used retrograde tracing to label RGCs and then count the labeled cells within the retina [4,5]. More recently, immunostaining for RGC specific markers was used to quantify RGCs in the mouse retina. This includes BRN3A immunolabeling [6] and RBPMS immunolabeling [7-9]. Retrograde labeling [4,10] is also used to identify RGCs. Most of these methods require manual counting to sample a limited area of the retina [2]. However, RGCs are not evenly distributed across the surface of the retina, with areas of relatively high density and low density of RGCs. As a result, the sampling of a few small regions of the retina could lead to considerable variability depending on if the sample is from a high RGC density region or a low RGC density region of the retina. This type of variability may be responsible in part for the differences in reported estimates of rodent RGCs that ranges from 36.1% to 59.8% for the C57BL/6J strain alone [3]. In the present study, when possible, we used automated counting methods to quantify RGCs across the entire retina [11].

The analysis of mouse RGCs becomes increasingly complicated with the RGC subtypes within the retina [12].

Correspondence to: Eldon E. Geisert, Department of Ophthalmology, Emory University, 1365B Clifton Road NE, Atlanta GA 30322; Phone: (404) 778-4239; email: egeiser@emory.edu

Table 1. All of the antibodies used in this study are listed.

Antibodies	Dilution	Source	Identifier
Rabbit anti-POU6F2	1:500	MyBiosource	Cat. #MBS9402684
Rabbit anti-BRN3A	1:500	Synaptic Systems	Cat. #411003
Mouse anti-BRN3A	1:500	Santa Cruz	Cat. #sc-8429
Mouse anti-SATB2	1:500	Abcam	Cat. #ab51502
Rabbit anti-OPN4	1:500	Advanced Targeting Systems	Cat. #AB-N39
Mouse anti-SMI32	1:500	BioLegend	Cat. #801701
Donkey anti-mouse, Alexa Fluor 488 conjugated	1:1000	Jackson Immunoresearch	Cat. #715–545–150
Donkey anti-mouse, Alexa Fluor 594 conjugated	1:1000	Jackson Immunoresearch	Cat. #715–585–150
Donkey anti-rabbit, Alexa Fluor 488 conjugated	1:1000	Jackson Immunoresearch	Cat. #715–545–152
Donkey anti-rabbit, Alexa Fluor 594 conjugated	1:1000	Jackson Immunoresearch	Cat. #711–585–152

Investigation of the different RGC subtypes reveals selective sensitivity to injury [13-17]. For example, some cell types like POU6F2-positive RGCs are selectively sensitive to glaucoma [14,15], while other RGC subtypes are resistant to injury like the intrinsically photosensitive RGCs [18]. This variability can affect interpretation of results of total ganglion cell loss when evaluating factors such as neuroprotection or regeneration in the eye. We have recently found that a combination of POU6F2 and BRN3A immunostaining labels the nuclei of all RGCs in the mouse, facilitating the use of automated counting methods to quantify total RGCs in the retina [11]. This method measures cells across the entire retina and eliminates the potential underestimation of RGC counts using the traditional RBPMS or BRN3A markers alone. The present study uses POU6F2 and BRN3A immunostaining to quantify the total RGCs across six different inbred mouse strains.

METHODS

Mice: Mouse lines were chosen to obtain a cross section of mice of varying genetic backgrounds. Six strains of mice, including 129X1/SvJ, A/J, BALB/cByJ, C57BL/6J, CBA/CaJ, and CAST/EiJ, were chosen to represent mice from the Castle's, Bagg Albino, C57-related, and wild-derived strain lines. None of the strains selected are known to express any mutations resulting in retinal degeneration. All mice were purchased from The Jackson Laboratory and housed in a pathogen-free facility at Emory University, maintained on a 12h:12h light-dark cycle, provided with food and water ad libitum. Between 55 and 70 days of age, the mice were deeply anesthetized with a mixture of ketamine 100 mg/kg and xylazine 10 mg/kg and then perfused through the heart with Phosphate Buffered Saline (PBS), followed by 4% paraformaldehyde in phosphate buffer (pH 7.3). The eyes were removed, and the retinas were dissected out. All procedures involving animals were approved by the Institutional Animal Care and Use Committee of Emory University and were in accordance with the ARVO Statement for the Use of Animals in Ophthalmic and Vision Research.

Immunohistochemistry: Flat mounts of the retina were prepared for staining using a similar protocol to what was previously described [11]. The retinas were blocked in 3% BSA and 3% donkey serum in 0.5% Triton X-100 in PBS. Retinas were stained with combinations of primary antibodies over two nights at 4 °C, then rinsed three times with PBST (0.1% Tween-20 in PBS) for 15 min each and placed in secondary antibodies overnight. The retinas were then rinsed three more times with PBST for 15 min each, and counterstained with TO-PRO-3 (Thermo Fisher Scientific, Cat. #T3605, Waltham, MA) at 1:1500 for 10 min. Finally, the retinas were rinsed with PBS three times for 15 min each before being mounted on glass slides. All antibodies and concentrations used are presented in Table 1.

Retinas from each strain (a total of six mice per strain) were stained with three different combinations of primary and secondary antibodies. The first set of retinas (n=4) were stained for rabbit anti-POU6F2 (MyBioSource, Cat. #MBS9402684, San Diego, CA), rabbit anti-BRN3A (Synaptic Systems, Cat. #411003, Goettingen, Germany), mouse anti-SATB2 (Abcam, Cat. #AB51502, Waltham, MA) and counterstained with TO-PRO-3 (Thermo Fisher Scientific, Cat. #T3605). The second set of retinas (n=4) were stained with rabbit anti-OPN4 (Advanced Targeting Systems, Cat. #AB-N39, Carlsbad, CA), mouse anti-SMI32 (BioLegend, Cat. #801701, San Diego, CA) and counterstained with TO-PRO-3 (Thermo Fisher Scientific, Cat. #T3605). The third set of retinas (n=4) were stained with rabbit anti-POU6F2, mouse anti-BRN3A (Santa Cruz, Cat. #sc-8429, Dallas, TX) counterstained with TO-PRO-3 (Thermo Fisher Scientific, Cat. #T3605). Retinal flat mounts were imaged with a Nikon Eclipse TI confocal microscope (Nikon, Inc.

Melville, NY) under a 20X magnification. The microscope is focused on the retinal flat mount at low magnification and then images are systematically tiled across the retina with a 60 µm Z-stack with 2.5µm steps. Stitching of individual fields was done using NIS Elements software. A maximum intensity projection through the stack is used to create a 2D image of the flatmount.

Automated counting: RGCode, a deep learning tool for automated detection and quantification of murine RBPMS-immunopositive RGCs, was used to calculate the global number of RGCs in the ganglion cell layer (GCL). This tool was also used to calculate the number of POU6F2, BRN3A, and SATB2 positive cells that were immunolabeled in the GCL. Detailed descriptions of this tool can be found in the original literature [19], and the code is available for download at GitLab. Though RGCode was initially designed to detect $RBPMS^+$ RGCs, it was successfully tested in our previous study to accurately count POU6F2, BRN3A, and a combination of BRN3A and POU6F2 labeled cells as a pan-RGC marker [11]. FIJI (ImageJ), an open-source platform for biologic-image analysis, was used in the quantification of total nuclei in the GCL as labeled by TO-PRO-3 [20]. RGCode defines the area of the entire retina, counts total RGCs and determines the spatial density of RGCs across the retina [19].

Manual counting: Melanopsin (OPN4) positive cells were counted manually using the FIJI software. Grids of size 500,000 μm^2 were created throughout each image. One grid was selected for counting from each quadrant of the dissected retina to account for the uneven dorsoventral distribution of OPN4 cells across the mouse retina [21]. The counts from the four quadrants were averaged to calculate the estimated density of OPN4-positive cells in the GCL. SMI32-positive cells were counted in a similar manner, but with grids of size 311,364 μm^2. The counts from four quadrants were averaged to calculate the estimated density of each cell type per μm^2.

Statistical analysis: Data are presented as Mean ± SEM (standard error). Differences in cell counts were analyzed by the Kruskal-Wallis H test using SPSS (Statistical Package for the Social Sciences) statistical package 24.0 (SPSS, IBM, Chicago, IL). A value of $p<0.05$ was considered statistically significant.

RESULTS

Different strains of inbred mice are used to study RGCs in vision research, and in general, we assume that the number of RGCs and RGC subtypes are similar across the different mouse strains. To determine if the RGC populations in different mouse inbred strains are similar, we examined six commonly used mouse strains: 129X1/SvJ, A/J, BALB/cByJ, C57BL/6J, CAST/EiJ and CBA/CaJ. The number of RGCs in six strains was examined using immunohistochemical methods. We also quantified the number of specific RGC subtypes in these strains. An estimate of displaced amacrine cells was made by taking the total number of nuclei in the ganglion cell layer and subtracting the number of immunostained RGCs.

Four retinas from each strain were stained for BRN3A, POU6F2, and counterstained with TO-PRO-3 to label all nuclei in the ganglion cell layer. In a previous study [11], we demonstrated that the combination of BRN3A labeling and POU6F2 labeling marks the nuclei of all RGCs that are positive for RBPMS (a pan-RGC marker [10]). Some RGCs are positive for both markers RBPMS and BRN3A [11]. When we examine the distribution of labeled RGCs across the retina, it is clear that there are regions of high density of labeled RGCs and regions of low density of RGCs (Figure 1). This regional variation in RGC density displays the need to count the number of RGCs across the entire retina and not depend on random sampling of small regions to calculate the total RGC number. In the present study, we used automated counting procedures to define the total number of RGCs in each mouse retina [11,19]. The pattern of immunostaining for BRN3A and POU6F2 for all 6 strains of mice is illustrated in Figure 2. The overall density of RGC nuclei in each of the retinas appears to be similar. However, upon closer examination, it appears that some strains like CAST/EiJ and BALB/cByJ have qualitatively fewer RGCs than other strains such as C57BL/6J and 129X1/SvJ. In addition, the density of some of the RGC subtypes appears to vary. For example, the POU6F2-positive RGCs (red) and the BRN3A-positive RGCs (green) differ between the various mouse strains. In the A/J strain (Figure 2), there appears to be fewer POU6F2-positive RGCs relative to the BALB/cByJ strain (Figure 2). Also, the number of BRN3A-positive cells appears to be high in C57BL/6J and low in CAST/EiJ. To quantify the differences in total RGC number as well as RGC subtype number, we used automated counting of the entire retina. Nuclear labeling facilitates automated counting, providing for an accurate determination of RGC cell types. The retinal counts for all 6 strains of mice are presented in Table 2. The strain with the highest number of BRN3A-positive RGCs is the C57BL/6J strain with an average of 44,253 cells per retina. The strain with the lowest number of BRN3A-positive RGCs is the CAST/EiJ strain with an average of 34,572 cells per retina. This represents a surprising 22% difference (significant, $p<0.01$) in the number of BRN3A-positive RGCs (Figure 2). When we examined the RGCs positive for POU6F2, the strain with the highest number of POU6F2-positive RGCs is the BALB/cByJ strain with an average of 27,092 cells per retina, and the strain

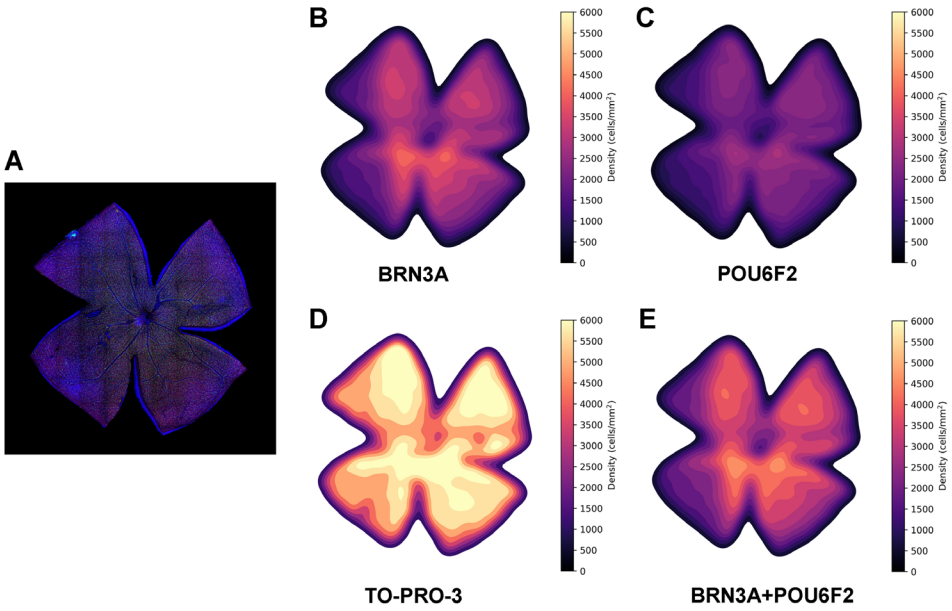

Figure 1. The density of RGC subtypes varies across the surface of the retina. **A** is a retinal flat mountstained for BRN3A, POU6F2, and counterstained for TO-PRO-3. The density of the BRN3A-positive RGCs across the retina is shown in **B**. The density of the POU6F2-positive RGCs is shown in **C**. The density of TO-PRO-3 positive nuclei is shown in **D. E** displays the distribution of total RGCs (a combination of BRN3A and POU6F2 staining). The density is shown as a heat map with the color scale to the right of each image indicating cell number and matching color.

with the lowest number was A/J with an average of 15,812 of these RGCs per retina (significant, $p<0.001$). This was an even greater difference than observed in the BRN3A-positive RGCs, with a 42% difference in POU6F2-positive cells.

To define the total number of RGCs in the different strains, we double stained the retina for both BRN3A and POU6F2. Previously, we demonstrated that the combination of BRN3A and POU6F2 labels all RGCs that are RBPMS-positive. There are multiple lines of evidence that RBPMS labels all RGCs in the mouse retina. Tran et al. [12] shows that the mRNA for RBPMS is expressed in all retinal ganglion cell types at relatively high levels. Furthermore, using RBPMS to label RGCs in the retina of mice that have been retrogradely labeled with Fluorogold, Kong et al. [10] demonstrated that virtually all RGCs labeled with the RBPMS antibody were also positive for Fluorogold. Thus, RBPMS labels virtually all RGCs in the mouse. When we examined retinas stained for both BRN3A and POU6F2, many of these cells were positive for both markers (Figure 2). The nuclear staining of these two markers allows us to use automated counting programs to identify the total number of RGCs in a retina (Figure 3). Looking at the total number of RGCs per strain, the strain with the highest number of RGCs was the 129X1/SvJ strain with an average of 53,872 RGCs per retina. The strain with the lowest number of RGCs was the CAST/EiJ strain with 39,961 RGCs per retina. These data reveal there is a significant difference ($p<0.01$) in the number of RGCs per retina in the different strains of mice (Table 2). These numbers are confounded to some extent by differences in the size of the retinas. The strain with the largest retina was the CBA/CaJ strain with a retinal area of 14.73 mm^2 and the strain with the smallest retina was the CAST/EiJ strain with an area of 12.97 mm^2. If we look at the density of RGCs across the strains, the range narrows. The strain with the highest density is 129X1/SvJ with an average of 3769 cells per mm^2 and the strain with the lowest density is the CAST/EiJ strain with an average of 3087 RGCs per mm^2. This represents an 18% difference in RGC density across the strains, indicating that the large difference observed in total RGCs is due in part to differences in retinal area. In the present study, we have not made an attempt to include RGCs that are displaced in the inner nuclear layer.

Many of the cells in the ganglion cell layer of the mouse retina are actually displaced amacrine cells. The displaced amacrine cells make up approximately 50% of the nuclei in this layer. To provide an estimate of the number of RGCs relative to the number of displaced amacrine cells across the different strains of mice, we stained the retinas for BRN3A and POU6F2 to label all RGCs and counterstained the retinas with TO-PRO-3 to label all nuclei within the ganglion cell layer. The total number of nuclei in the retinas ranged from 104,602 nuclei in the C57BL/6J strain to 86,764 nuclei in the BALB/cByJ strain (Table 2). We are using this number to calculate the number of displaced amacrine cells, even though some of these nuclei are non-neuronal cells, including endothelial nuclei and astrocyte nuclei. Using the total number of RGCs per strain and the total number of nuclei per strain, we estimated the percentage of displaced amacrine cells for

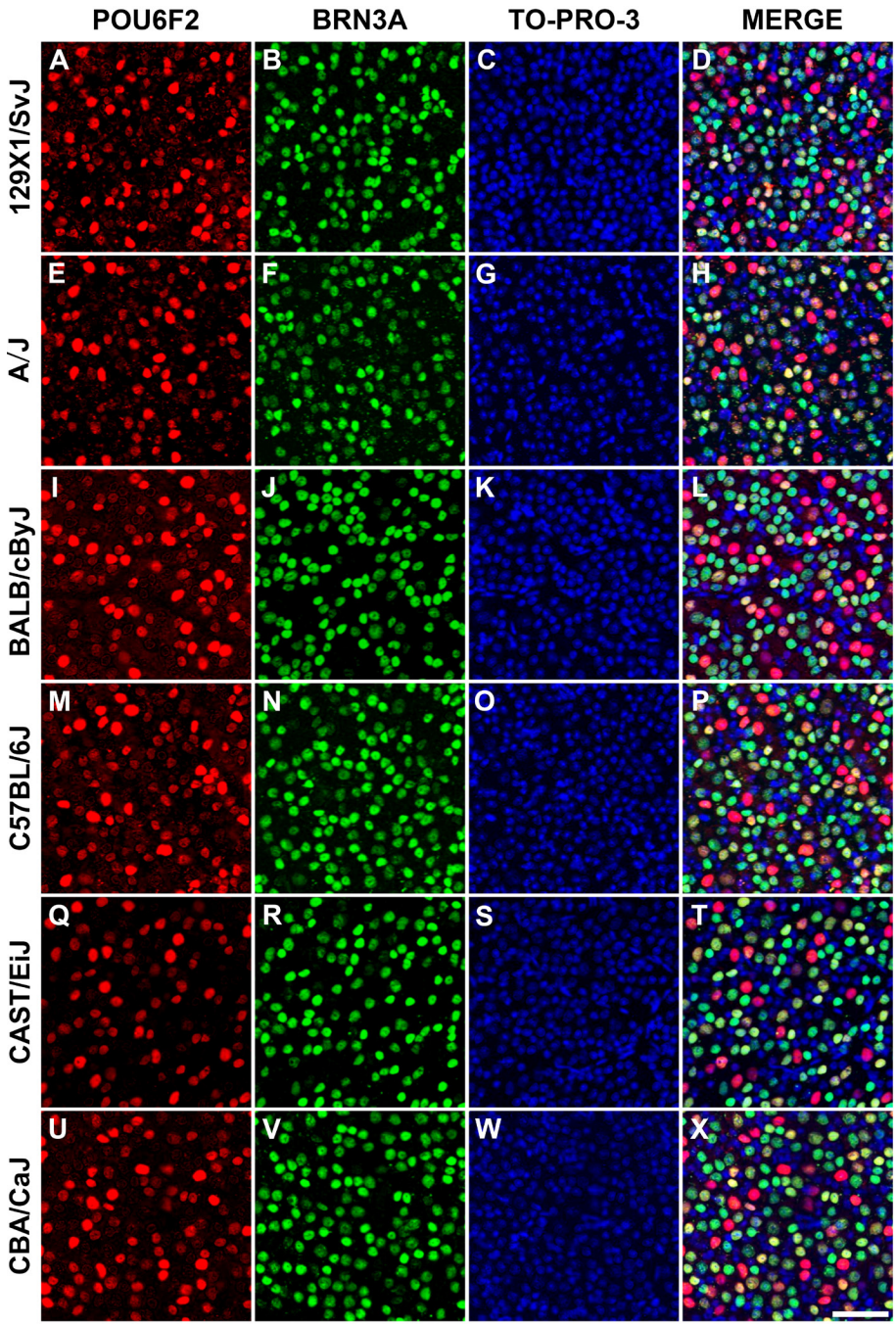

Figure 2. Photomicrographs from stained retinas are shown for all six strains of mice used in this study: 129X1/SvJ, A/J, BALB/cByJ, C57BL/6J, CBA/CaJ, and CAST/EiJ. The retinas stained for POU6F2 (red, **A**, **E**, **I**, **M**, **Q** and **U**) and BRN3A (green, **B**, **F**, **J**, **N**, **R** and **V**). The retinas were counter strained with TO-PRO-3 (blue, **C**, **G**, **K**, **O**, **S** and **W**) to label all of the nuclei in the retinal ganglion cell layer. Merged images of all three channels are shown (**D**, **H**, **L**, **P**, **T** and **X**). Notice that some strains have higher numbers of POU6F2 RGCs (BALB/cByJ) while other strains have relatively few POU6F2 RGCs (CAST/EiJ). Scale bar in X equals 50 µm.

Table 2. The number of different populations of RGCs is presented.

Mouse strain	C57BL/6J	BALB/cByJ	129×1/SvJ	A/J	CBA/CaJ	CAST/EiJ
BRN3A (cells/retina)	44,253±798	40,977±484	42,866±983	36,184±1604	43,381±957	34,572±494
POU6F2 (cells/retina)	21,816±131	27,093±791	18,777±1043	15,812±740	23,799±1391	20,795±421
Total RGCs (cells/retina)	52,037±555	43,580±1167	53,872±1864	44,693±609	50,607±935	39,961±838
Total nuclei (cells in GCL)	104,603±702	86,764±323	112,964±950	87,074±994	102,945±2272	89,463±536
RGC/Total nuclei (%)	49.7±0.5	50.2±1.3	47.7±1.6	51.3±0.7	49.2±0.9	44.7±0.9
SATB2 (cells/retina)	11,160±278	9944±384	13,772±432	14,001±1141	15,872±1196	9645±821
OPN4 density (cells/mm^2)	119±5	126±8	164±13	124±4	115±5	110±7
SMI32 density (cells/mm^2)	279±12	202±15	203±8	183±14	244±34	203±21
Retina area (mm^2)	14.4±0.5	13.0±0.5	14.3±0.5	14.0±0.1	14.7±0.3	13.0±0.2

The data for all 6 strains of mice examined are presented with the Mean ± SEM. The data was collected from 4 retinas for each strain.

each of the strains by subtracting the total number of RGCs from the total number of nuclei (Table 2). Interestingly, even though the total number of RGCs in each strain was quite different, the percentage of RGCs per strain was relatively similar with the highest percentage being 51.33% in the A/J strain and the lowest percentage being 44.67% in the CAST/EiJ strain. The difference in the percentage of RGCs was only 13%. Thus, even though the number of RGC varied considerably between strains, the ratio of RGC to amacrine cells was similar across the six mouse strains examined.

A sampling of other RGC subtypes was also examined in each of the strains. We looked at SATB2, a transcription factor known to be expressed in ON-OFF directionally selective (ooDS) RGCs in the mouse [22-24]. There was a surprising difference in the number of SATB2-positive RGCs between the 6 strains of mice (Table 2). The strain with the highest number of SATB2-positive RGCs was CBA/CaJ with on average 15,872 RGCs per retina. The strain with the lowest number of SATB2-positive RGCs was CAST/EiJ with an average of only 9,645 RGCs per retina. This represents a surprising 61% difference between these two strains. This difference may be due in part to the fact that we observed considerably fewer RGCs in the CAST/EiJ strain (39,961 RGCs per retina) relative to the number of RGCs in the 129X1SvJ strain (53,872 RGCs per retina). If we examine the percentage of SATB2-positive RGCs relative to total RGCs (Table 2), the difference between the strains is considerably less. The strains with the highest percentage of SATB2 RGCs are the A/J and CBA/CaJ strains with a percentage of 32% each. The strain with the lowest percentage of SATB2 cells is C57BL/6J with only 21%. This still represents a relatively large difference in SATB2-positive RGCs.

The final two RGC subtypes examined were OPN4-positive cells known to be intrinsically photosensitive RGCs and SMI32 (neurofilament heavy chain) positive RGCs which marks the large alpha RGCs. For both these cell types, it was not possible to use automated counting of the entire retina, due to the staining of axons and dendrites which complicated the process. For the quantification of OPN4, we chose 4 fields (707 × 707 µm) and counted the numbers of cells in the fields to determine cell density (see Table 2). For the quantification of SMI32, we chose 4 fields of size 558×558 µm and calculated the density in the same manner as OPN4. For OPN4-positive RGCs, there was a 32% difference cell density across all strains with the lowest strain being CAST/EiJ (110 cells/mm^2) and the highest strain being 129×1/SvJ (164 cells/mm^2). For the SMI32-positive RGCs, there was a 34% difference across all 6 strains, with the lowest strain being A/J (183 cells/mm^2) and the strain with the highest density being C57BL/6J (279 cells/mm^2).

DISCUSSION

RGCs are the final common pathway for propagating visual stimuli from the retina to the brain. RGC damage or loss can result from injury [25,26], degenerative conditions such as glaucoma [27-29], or inherited disease [30]. This loss of RGCs is often associated with loss of vision [31]. Mouse models are widely used in vision research to study factors that influence RGC death and survival. Most of these mouse models use inbred mouse strains that were developed by inbreeding over many generations. Thus, each of these inbred strains offers a unique genetic background that could potentially have significant influence on the experimental outcomes.

There is a long history associated with inbred mouse strains beginning with the DBA mouse developed by C.C. Little in 1909 [32]. The DBA mouse was initially an experiment in eugenics that produced a mouse susceptible for developing cancer. It proved to be a pivotal milestone

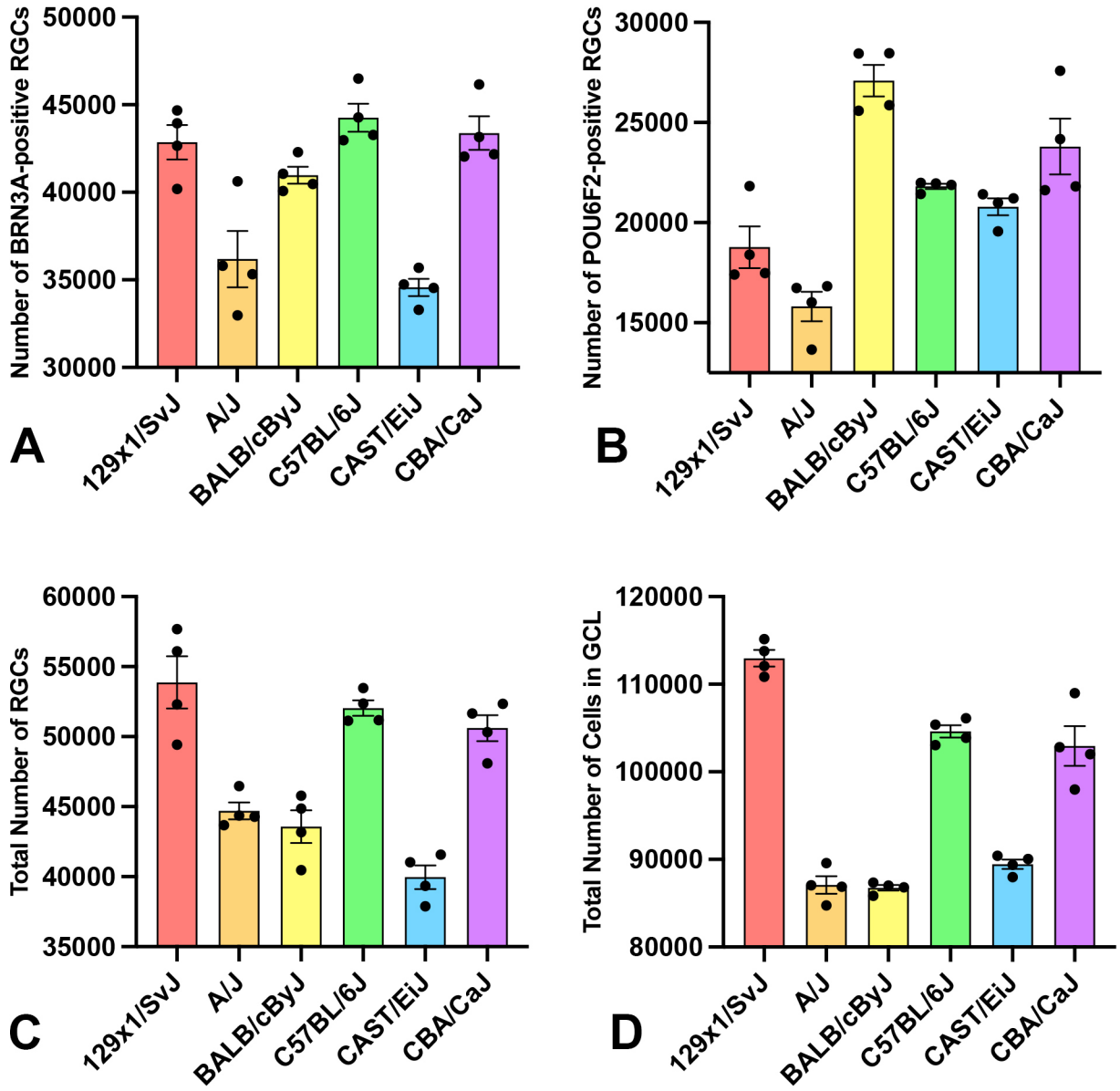

Figure 3. The number of RGC in six different inbred strains (129×1/SvJ, A/J, BALB/cByJ, C57BL/6J, CBA/CaJ, and CAST/EiJ) of mice is shown in four bar graphs. Each bar represents the mean number with the standard error of the mean indicated by brackets. **A** displays the number of BRN3A-positive RGCs. The number of POU6F2- positive RGCs is shown in **B**. The total number of RGCs is shown in **C** and the total number of cells in the ganglion cell layer (GCL) is shown in **D**.

in cancer research. Since the initial production of the DBA inbred mouse strain, many different strains were developed and used throughout biology [33]. Most of these inbred strains were produced with the intention of developing specific phenotypes. Thus, when examining RGCs in different inbred strains, it is not expected to find mice that were intentionally bred to have refined vision, or that perform better on visually guided tasks. In fact, many inbred strains are blind and this phenotype was not realized until the retinas were examined and found to lack photoreceptors. Examples of this include mouse strains such as C3H, CBA, FVB/N that carry the rd1 mutation [34]. These mice were bred for many generations before it was noticed that their retinas lacked photoreceptors due to the rd1 mutation [34-36]. This is just one example of a phenotype that occurred during the inbreeding process and subsequent breeding across the generations of specific mouse strains. It is also the consequence of the fact that in

inbred strains the parental alleles are identical, resulting in the expression of what would normally be recessive traits.

Another example of a non-intentional phenotype in selected inbred mouse strains comes from the Nickells' laboratory [37]. They examined the susceptibility of RGCs to optic nerve crush (ONC) in 15 different mouse strains. There were significant differences in neuronal death between the different strains. The strain most resistant to optic nerve crush was the DBA/2J mouse and the strain most susceptible of optic nerve crush was the BALB/cByJ mouse. This demonstrates the effects of different genetic backgrounds on RGC susceptibility to injury. One potential source for the differential effects of optic nerve crush across mouse strains is differences in the molecularly-identified RGC subtypes within individual strains of mice. In the mouse retina, there are 46 RGC subtypes [12]. Different RGC subtypes vary in their susceptibility to injury (for review see [13]). Some RGC subtypes are very susceptible to injury and many of these cells are ON-OFF directionally selective RGCs [15-17,28]. Other RGC subtypes are resistant to injury and include alpha RGCs [16,17] and intrinsically photosensitive RGCs [12,38]. Interestingly, of the 15 strains studied in the Nickells laboratory, the most sensitive strain to optic nerve crush was the BALB/cByJ mouse, and this strain has the highest percentage of POU6F2-positive RGCs that are known to be susceptible to glaucomatous damage [39].

RGC subtypes have significantly different responses to ONC with many being very susceptible to the injury [16,37], while others are relatively resistant, like the alpha RGCs including the M1 subclass [12,38,40]. This is also seen in mouse glaucoma models where the M1 RGCs survive glaucoma induced by photocoagulation [41]. In the *nee* mouse model of glaucoma (caused by mutation of the *Sh3pxd2b* gene), there was a greater sensitivity of the TRHR-RGCs (a subset of ooDS RGCs) to injury than the OFF RGCs, or the M1 RGCs [28]. These findings reveal that the choice of the mouse strain used in studies in RGCs is critical and can potentially affect the outcome of the experiment.

Finally, one of the striking findings from our study is the relative consistency of the number of RGCs relative to the number of amacrine cells (non-RGCs in the ganglion cell layer). Within the ganglion cell layer, the percentage of RGCs (labeled by POU6F2 and BRN3A) ranges from 44.7% to 51.3%. This finding suggests that there are conserved developmental processes that regulate the percentage of displaced amacrine cells relative to the number of RGCs.

While the present study establishes a robust quantitative framework for total RGC and RGC subtype distributions across several widely used inbred mouse strains, additional studies are required to extend these findings to a broader range of genetic backgrounds. In particular, for disease-relevant mouse models used in glaucoma, optic nerve injury, and inherited retinal degeneration research, strain dependent baseline differences in RGC and RGC subtype composition may influence disease susceptibility, progression, and therapeutic response. The functional consequences of these strain-dependent differences in RGC distributions on visual processing, retinal physiology, or disease susceptibility also remains unknown, and will require further investigation. Future studies incorporating larger sample sizes, longitudinal analysis, and functional assessments will be important to determine how these anatomic differences translate into visual performance and vulnerability to retinal disease.

In conclusion, by quantifying RGC subtypes across six commonly used inbred mouse strains, our study establishes a reference framework for baseline RGC composition in the mouse retina. These data highlight the importance of genetic background as a biologic variable in retinal research, particularly for models of glaucoma, optic nerve injury, and retinal degeneration. Awareness of strain-dependent differences in RGC subtype distribution will aid in the interpretation of experimental outcomes and the selection of appropriate mouse lines for future mechanistic and therapeutic studies.

ACKNOWLEDGMENTS

The authors would like to thank Micah Chrenek for his technical assistance in this study. Authors contributions: The following are the authors contribution to the publication: design of experiments (JW, S-TL, FL, EEG), provide funding (EEG), collection and analysis of data (JW, EEG), writing the manuscript (EEG), and making substantial edits to the manuscript (FL, S-TL, EEG). Funding: This study was supported by two grants from NEI grant R01EY031042 (E.E.G.), P30EY06360 (Emory Vision Core), a Challenge Grant from Research to Prevent Blindness and a gift from the Owens Family Glaucoma Research Fund. Conflict of Interest The authors declare that they have no competing interests.

REFERENCES

1. Jeon CJ, Strettoi E, Masland RH. The major cell populations of the mouse retina. J Neurosci 1998; 18:8936-46. [PMID: 9786999].

2. Williams RW, Strom RC, Rice DS, Goldowitz D. Genetic and environmental control of variation in retinal ganglion cell number in mice. J Neurosci 1996; 16:7193-205. [PMID: 8929428].

3. Schlamp CL, Montgomery AD, Mac Nair CE, Schuart C, Willmer DJ, Nickells RW. Evaluation of the percentage of

ganglion cells in the ganglion cell layer of the rodent retina. Mol Vis 2013; 19:1387-96. [PMID: 23825918].

4. Pang JJ, Wu SM. Morphology and immunoreactivity of retrogradely double-labeled ganglion cells in the mouse retina. Invest Ophthalmol Vis Sci 2011; 52:4886-96. [PMID: 21482641].

5. Dräger UC, Olsen JF. Ganglion cell distribution in the retina of the mouse. Invest Ophthalmol Vis Sci 1981; 20:285-93. [PMID: 6162818].

6. Davis BM, Guo L, Brenton J, Langley L, Normando EM, Cordeiro MF. Automatic quantitative analysis of experimental primary and secondary retinal neurodegeneration: implications for optic neuropathies. Cell Death Discov 2016; 2:16031-[PMID: 27551521].

7. Kwong JM, Caprioli J, Piri N. RNA binding protein with multiple splicing: a new marker for retinal ganglion cells. Invest Ophthalmol Vis Sci 2010; 51:1052-8. [PMID: 19737887].

8. Rodriguez AR, de Sevilla Müller LP, Brecha NC. The RNA binding protein RBPMS is a selective marker of ganglion cells in the mammalian retina. J Comp Neurol 2014; 522:1411-43. [PMID: 24318667].

9. Meng M, Chaqour B, O'Neill N, Dine K, Sarabu N, Ying GS, Shindler KS, Ross AG. Comparison of Brn3a and RBPMS Labeling to Assess Retinal Ganglion Cell Loss During Aging and in a Model of Optic Neuropathy. Invest Ophthalmol Vis Sci 2024; 65:19-[PMID: 38587440].

10. Kwong JM, Quan A, Kyung H, Piri N, Caprioli J. Quantitative analysis of retinal ganglion cell survival with Rbpms immunolabeling in animal models of optic neuropathies. Invest Ophthalmol Vis Sci 2011; 52:9694-702. [PMID: 22110060].

11. Lin F, Lin ST, Wang J, Geisert EE. Optimizing retinal ganglion cell nuclear staining for automated cell counting. Exp Eye Res 2024; 242:109881[PMID: 38554800].

12. Tran NM, Shekhar K, Whitney IE, Jacobi A, Benhar I, Hong G, Yan W, Adiconis X, Arnold ME, Lee JM, Levin JZ, Lin D, Wang C, Lieber CM, Regev A, He Z, Sanes JR. Single-Cell Profiles of Retinal Ganglion Cells Differing in Resilience to Injury Reveal Neuroprotective Genes. Neuron 2019; 104:1039-1055.e12. [PMID: 31784286].

13. Tapia ML, Nascimento-Dos-Santos G, Park KK. Subtype-specific survival and regeneration of retinal ganglion cells in response to injury. Front Cell Dev Biol 2022; 10:956279[PMID: 36035999].

14. King R, Struebing FL, Li Y, Wang J, Koch AA, Cooke Bailey JN, Gharahkhani P, MacGregor S, Allingham RR, Hauser MA, Wiggs JL, Geisert EE. International Glaucoma Genetics Consortium; NEIGHBORHOOD Consortium. Genomic locus modulating corneal thickness in the mouse identifies POU6F2 as a potential risk of developing glaucoma. PLoS Genet 2018; 14:e1007145[PMID: 29370175].

15. Lin F, Li Y, Wang J, Jardines S, King R, Chrenek MA, Wiggs JL, Boatright JH, Geisert EE. POU6F2, a risk factor for glaucoma, myopia and dyslexia, labels specific populations of retinal ganglion cells. Sci Rep 2024; 14:10096-[PMID: 38698014].

16. Daniel S, Clark AF, McDowell CM. Subtype-specific response of retinal ganglion cells to optic nerve crush. Cell Death Discov 2018; 4:7-[PMID: 30062056].

17. VanderWall KB, Lu B, Alfaro JS, Allsop AR, Carr AS, Wang S, Meyer JS. Differential susceptibility of retinal ganglion cell subtypes in acute and chronic models of injury and disease. Sci Rep 2020; 10:17359-[PMID: 33060618].

18. Cui Q, Ren C, Sollars PJ, Pickard GE, So KF. The injury resistant ability of melanopsin-expressing intrinsically photosensitive retinal ganglion cells. Neuroscience 2015; 284:845-53. [PMID: 25446359].

19. Masin L, Claes M, Bergmans S, Cools L, Andries L, Davis BM, Moons L, De Groef L. A novel retinal ganglion cell quantification tool based on deep learning. Sci Rep 2021; 11:702-[PMID: 33436866].

20. van der Heide CJ, Meyer KJ, Hedberg-Buenz A, Pellack D, Pomernackas N, Mercer HE, Anderson MG. Quantification and image-derived phenotyping of retinal ganglion cell nuclei in the nee mouse model of congenital glaucoma. Exp Eye Res 2021; 212:108774[PMID: 34597676].

21. Hughes S, Watson TS, Foster RG, Peirson SN, Hankins MW. Nonuniform distribution and spectral tuning of photosensitive retinal ganglion cells of the mouse retina. Curr Biol 2013; 23:1696-701. [PMID: 23954426].

22. Sweeney NT, James KN, Nistorica A, Lorig-Roach RM, Feldheim DA. Expression of transcription factors divides retinal ganglion cells into distinct classes. J Comp Neurol 2019; 527:225-35. [PMID: 28078709].

23. Peng YR, Tran NM, Krishnaswamy A, Kostadinov D, Martersteck EM, Sanes JR. Satb1 Regulates Contactin 5 to Pattern Dendrites of a Mammalian Retinal Ganglion Cell. Neuron 2017; 95:869-883.e6. [PMID: 28781169].

24. Dhande OS, Stafford BK, Franke K, El-Danaf R, Percival KA, Phan AH, Li P, Hansen BJ, Nguyen PL, Berens P, Taylor WR, Callaway E, Euler T, Huberman AD. Molecular Fingerprinting of On-Off Direction-Selective Retinal Ganglion Cells Across Species and Relevance to Primate Visual Circuits. J Neurosci 2019; 39:78-95. [PMID: 30377226].

25. Rodríguez-Ramírez KT, Norte-Muñoz M, Lucas-Ruiz F, Gallego-Ortega A, Calzaferri F, García-Bernal D, Martínez CM, Galindo-Romero C, de Los Ríos C, Vidal-Sanz M, Agudo-Barriuso M. Retinal response to systemic inflammation differs between sexes and neurons. Front Immunol 2024; 15:1340013[PMID: 38384465].

26. Dvoriantchikova G, Degterev A, Ivanov D. Retinal ganglion cell (RGC) programmed necrosis contributes to ischemia-reperfusion-induced retinal damage. Exp Eye Res 2014; 123:1-7. [PMID: 24751757].

27. Howell GR, Soto I, Libby RT, John SW. Intrinsic axonal degeneration pathways are critical for glaucomatous damage. Exp Neurol 2013; 246:54-61. [PMID: 22285251].

28. Daniel S, Meyer KJ, Clark AF, Anderson MG, McDowell CM. Effect of ocular hypertension on the pattern of retinal ganglion cell subtype loss in a mouse model of early-onset glaucoma. Exp Eye Res 2019; 185:107703[PMID: 31211954].

29. Nickells RW. The cell and molecular biology of glaucoma: mechanisms of retinal ganglion cell death. Invest Ophthalmol Vis Sci 2012; 53:2476-81. [PMID: 22562845].

30. Newman NJ, Carelli V, Taiel M, Yu-Wai-Man P. Visual Outcomes in Leber Hereditary Optic Neuropathy Patients With the m.11778G>A (MTND4) Mitochondrial DNA Mutation. J Neuroophthalmol 2020; 40:547-57. [PMID: 32969847].

31. Templeton JP, Nassr M, Vazquez-Chona F, Freeman-Anderson NE, Orr WE, Williams RW, Geisert EE. Differential response of C57BL/6J mouse and DBA/2J mouse to optic nerve crush. BMC Neurosci 2009; 10:90-[PMID: 19643015].

32. Castle WE, Little CC. The Peculiar Inheritance of Pink Eyes among Colored Mice. Science 1909; 30:313-4. [PMID: 17837461].

33. Mary F. Lyon. Genetic Variants and Strains of The Laboratory Mouse. 2nd ed., Oxford University Press; 1989.

34. Pittler SJ, Baehr W. Identification of a nonsense mutation in the rod photoreceptor cGMP phosphodiesterase beta-subunit gene of the rd mouse. Proc Natl Acad Sci U S A 1991; 88:8322-6. [PMID: 1656438].

35. Bowes C, Li T, Danciger M, Baxter LC, Applebury ML, Farber DB. Retinal degeneration in the rd mouse is caused by a defect in the beta subunit of rod cGMP-phosphodiesterase. Nature 1990; 347:677-80. [PMID: 1977087].

36. Ahuja P, Caffé AR, Ahuja S, Ekström P, van Veen T. Decreased glutathione transferase levels in rd1/rd1 mouse retina: replenishment protects photoreceptors in retinal explants. Neuroscience 2005; 131:935-43. [PMID: 15749346].

37. Li Y, Semaan SJ, Schlamp CL, Nickells RW. Dominant inheritance of retinal ganglion cell resistance to optic nerve crush in mice. BMC Neurosci 2007; 8:19-[PMID: 17338819].

38. Duan X, Qiao M, Bei F, Kim IJ, He Z, Sanes JR. Subtype-specific regeneration of retinal ganglion cells following axotomy: effects of osteopontin and mTOR signaling. Neuron 2015; 85:1244-56. [PMID: 25754821].

39. King R, Struebing FL, Li Y, Wang J, Koch AA, Cooke Bailey JN, Gharahkhani P, MacGregor S, Allingham RR, Hauser MA, Wiggs JL, Geisert EE. International Glaucoma Genetics Consortium; NEIGHBORHOOD Consortium. Genomic locus modulating corneal thickness in the mouse identifies POU6F2 as a potential risk of developing glaucoma. PLoS Genet 2018; 14:e1007145[PMID: 29370175].

40. Shoham Z, Zosmer A, Insler V. Early miscarriage and fetal malformations after induction of ovulation (by clomiphene citrate and/or human menotropins), in vitro fertilization, and gamete intrafallopian transfer. Fertil Steril 1991; 55:1-11. [PMID: 1898885].

41. Gao J, Griner EM, Liu M, Moy J, Provencio I, Liu X. Differential effects of experimental glaucoma on intrinsically photosensitive retinal ganglion cells in mice. J Comp Neurol 2022; 530:1494-506. [PMID: 34958682].

Articles are provided courtesy of Emory University and The Abraham J. & Phyllis Katz Foundation. The print version of this article was created on 20 February 2026. This reflects all typographical corrections and errata to the article through that date. Details of any changes may be found in the online version of the article.